ISSN 1674-1056
http://cpb.iphy.ac.cn
http://iopscience.iop.org/cpb
中国物理 B
Chinese Physics
中国物理 Chinese Physics B

Sputtered gold nanoparticles enhanced quantum dot light-emitting diodes

Abida Perveen, Xin Zhang(张欣), Jia-Lun Tang(汤加仑), Deng-Bao Han(韩登宝), Shuai Chang(常帅), Luo-Gen Deng(邓罗根), Wen-Yu Ji(纪文宇), Hai-Zheng Zhong(钟海政)

Citation: Chin. Phys. B . 2018, 27(8): 086101. **doi:** 10.1088/1674-1056/27/8/086101

Journal homepage: http://cpb.iphy.ac.cn; http://iopscience.iop.org/cpb

What follows is a list of articles you may be interested in

Facile and controllable synthesis of molybdenum disulfide quantum dots for highly sensitive and selective sensing of copper ions

Xue Li(李雪), Da-Wei He(何大伟), Yong-Sheng Wang(王永生), Yin Hu(胡音), Xuan Zhao(赵宣), Chen Fu(付晨), Jing-Yan Wu(吴静燕)

Chin. Phys. B . 2018, 27(5): 056104. **doi:** 10.1088/1674-1056/27/5/056104

Zn-Cu-codoped SnO_2 nanoparticles:Structural, optical, and ferromagnetic behaviors

Syed Zulfiqar, Zainab Iqbal, Jianguo Lü(吕建国)

Chin. Phys. B . 2017, 26(12): 126104. **doi:** 10.1088/1674-1056/26/12/126104

Label-free tungsten disulfide quantum dots as a fluorescent sensing platform for highly efficient detection of copper (II) ions

Xuan Zhao(赵宣), Da-Wei He(何大伟), Yong-Sheng Wang(王永生), Yin Hu(胡音), Chen Fu(付晨), Xue Li(李雪)

Chin. Phys. B . 2017, 26(6): 066102. **doi:** 10.1088/1674-1056/26/6/066102

Diffusion and thermite reaction process of film-honeycomb Al/NiO nanothermite: Molecular dynamics simulations using ReaxFF reactive force field

Hua-Dong Zeng(曾华东), Zhi-Yang Zhu(祝志阳), Ji-Dong Zhang(张吉东), Xin-Lu Cheng(程新路)

Chin. Phys. B . 2017, 26(5): 056101. **doi:** 10.1088/1674-1056/26/5/056101

Dual-blue light-emitting diode based on strain-compensated InGaN-AlGaN/GaN quantum wells

Yan Qi-Rong, Yan Qi-Ang, Shi Pei-Pei, Niu Qiao-Li, Li Shu-Ti, Zhang Yong

Chin. Phys. B . 2013, 22(2): 026102. **doi:** 10.1088/1674-1056/22/2/026102

SPECIAL TOPIC — Nanophotonics

Sputtered gold nanoparticles enhanced quantum dot light-emitting diodes*

Abida Perveen[1], Xin Zhang(张欣)[2], Jia-Lun Tang(汤加仑)[2], Deng-Bao Han(韩登宝)[2], Shuai Chang(常帅)[2,†], Luo-Gen Deng(邓罗根)[1], Wen-Yu Ji(纪文宇)[3], and Hai-Zheng Zhong(钟海政)[2,‡]

[1] *Department of Physics, Beijing Institute of Technology, Beijing* 100081, *China*
[2] *Department of Materials Science and Engineering, Beijing Institute of Technology, Beijing* 100081, *China*
[3] *Department of Physics, Jilin University, Changchun* 130023, *China*

(Received 30 December 2017; revised manuscript received 16 January 2018; published online 10 July 2018)

Surface plasmonic effects of metallic particles have been known to be an effective method to improve the performances of light emitting didoes. In this work, we report the sputtered Au nanoparticles enhanced electroluminescence in inverted quantum dot light emitting diodes (ITO/Au NPs/ZnMgO/QDs/TFB/PEDOT:PSS/Al). By combining the time-resolved photoluminescence, transient electroluminescence, and ultraviolet photoelectron spectrometer measurements, the enhancement of the internal field enhanced exciton coupling to surface plasmons and the electron injection rate increasing with Au nanoparticles' incorporation can be explained. Phenomenological numerical calculations indicate that the electron mobility of the electron transport layer increases from 1.39×10^{-5} cm^2/V·s to 1.91×10^{-5} cm^2/V·s for Au NPs modified device. As a result, the maximum device luminescence is enhanced by 1.41 fold (from 14600 cd/cm^2 to 20720 cd/cm^2) and maximum current efficiency is improved by 1.29 fold (from 3.12 cd/A to 4.02 cd/A).

Keywords: gold nanoparticles, plasmonic effect, quantum dots, light-emitting diodes

PACS: 61.46.Df, 73.20.Mf **DOI:** 10.1088/1674-1056/27/8/086101

1. Introduction

Quantum dots (QDs) present attractive features of precise emission bandwidth, saturated emission, tunable emission wavelengths, and high quality production with low cost solution processing.[1–5] Such promising features make QDs potential candidates for next-generation display technologies through fully functionalized quantum dot light emitting diodes (QD-LEDs).[6–10] Since the demonstration of first QD-LED in 1994, continuous efforts have been made to improve their performance and the device is comparable to conventional organic light-emitting diode in some performances.[2,3,11] In particular, the inverted device is suitable for the display due to the compatibility to the n-channel thin film transistor (TFT). The QD-LEDs still suffer low luminous efficiency and poor stability[12,13] due to imbalanced transportation and injection of carriers,[14] intrinsic photoluminescence (PL) quenching,[15] and weak out-coupling.[16,17]

Surface plasmons (SPs), which are collectively oscillating free electrons at the interface between metal and dielectric,[8,18] are being extensively investigated[10,14,19,20] and being preliminarily investigated in QD-LEDs.[21] Enhancements such as in PL[8,22] and internal quantum efficiency (IQE)[19] of electroluminescent (EL) devices have been demonstrated. Furthermore, localized surface plasmons (LSPs) associated with noble metal nanostructures show resonance coupling to excitons, providing the enlargement of local electromagnetic field, which results in a rapid radiative emission rate by effective energy coupling from QDs to LSPs.[8,23] Metal nanostructures have been previously made[3] and incorporated by chemical or thermal vapor deposition of thin films with post annealing at high temperature,[1] by spin coating,[24] or by patterned templates.[16] However, most of the methods to incorporate plasmonic metal nanostructures require a complicated process and they are sometimes incompatible with solution processed device applications.

Here in this paper, the direct sputtering of gold nanoparticles (Au NPs) on ITO substrate is proposed for improving the QD-LEDs. The generated Au NPs's layer creates a plasmonic effect without damaging soft or thin underlying organic films,[25] and thus contributing to not only increasing the work function of the electron transport layer, but also quickly injecting the electrons into QDs and rapidly coupling excitons to LSPs.

2. Experimental section

2.1. Preparation of Au NP film

Au target film was set to be 5 cm above the aimed substrate. The chamber was evacuated to 10 Pa and the sputtering

*Project supported by the National Natural Science Foundation of China (Grant Nos. 21603012, 61735004, and 61722502).
†Corresponding author. E-mail: schang@bit.edu.cn
‡Corresponding author. E-mail: hzzhong@bit.edu.cn
© 2018 Chinese Physical Society and IOP Publishing Ltd

process was initiated at 10 mA with various time spans of 5 s, 10 s, 20 s, and 30 s, separately. Then the sputtered Au films were annealed at 280 °C for 20 min to form discrete NPs.

2.2. Device fabrication

Mg-doped ZnO (ZnMgO) was spin-coated on the ITO substrate at 2000 rpm for 60 s and annealed at temperature 110 °C for 20 min. CdSe quantum dots were dispersed in n-heptane with a concentration of 30 mg/ml and spin-coated at 2500 rpm for 60 s, followed by heating to 90 °C for 10 min. Hole transport layer poly(9,9-dioctylfluorene-co-N-(4-(3-methylpropyl))diphenylamine) (TFB) was prepared in chlorobenzene and spun-coated at 4000 rpm for 30 s and annealed at 150 °C for 30 min, followed by spin coating of PEDOT:PSS at 4000 rpm for 60 s and baked at 160 °C for 15 min. Finally, 100-nm Al is thermally evaporated as an electrode.

2.3. Characterizations

Scanning electron microscopy (SEM) images and energy dispersive spectra (EDS) were taken on an S-4800 microscope (Hitachi, Ltd., Japan). Ultraviolet–visible spectroscopy (UV-Vis) absorption spectra of QDs' solutions were measured on a UV-6100 spectrophotometer and PL spectra were obtained using an F-380 fluorescence spectrometer. Current density–voltage (J–V) characteristics of QD-LEDs were measured using a Keithley 2400 power source analyzer. The luminance was measured using a spectroradiometer (Photo Research Inc. PR-655). Time-resolved photoluminescence (TRPL) measurement was collected using a fluorescence lifetime measurement system (Edinburgh FL920) at an excitation wavelength of 405 nm. Time-resolved electroluminescence (TREL) was carried out by applying a pulsed voltage to the device, then the output signal was collected by an avalanche photo diode (APD) detector (Hamamatsu C10508-01) and output to a digital oscilloscope (Tektronix DPO7104C). Ultraviolet photoelectron spectrometry (UPS) was carried out on an ESCALAB 250XI XPS Microprobe (with a UV source accessory, ThermoFisher Scientific) using He Iα photon energy (21.22 eV).

3. Results and discussion

The corresponding SEM micrograph of optimized sputtered substrate after thermal annealing is shown in Figs. 1(a) and Fig. S1 (see Appendix A). It can be clearly seen that spherical Au NPs with an average size of 22 nm (20-s sputtering time) are uniformly distributed over the entire surface of ITO. The changes in the size of as-prepared Au NPs are found to be 12 nm, 13.5 nm, 22 nm, and 35 nm, corresponding to the variations of sputtering time. Figure 1(b) shows the size-dependent extinction characteristics of Au NPs on ITO substrates and the PL spectra of QD film. Size dependent absorption of Au NP film is observed and the absorption of non-annealed continuous sputtered metal film shows no plasmonic resonance absorption peak. The PL emission peak of QD at a wavelength of 518 nm matches perfectly with an absorption peak of 22-nm Au NP film, which indicates highly efficient coupling of excitons to the SPs.[9]

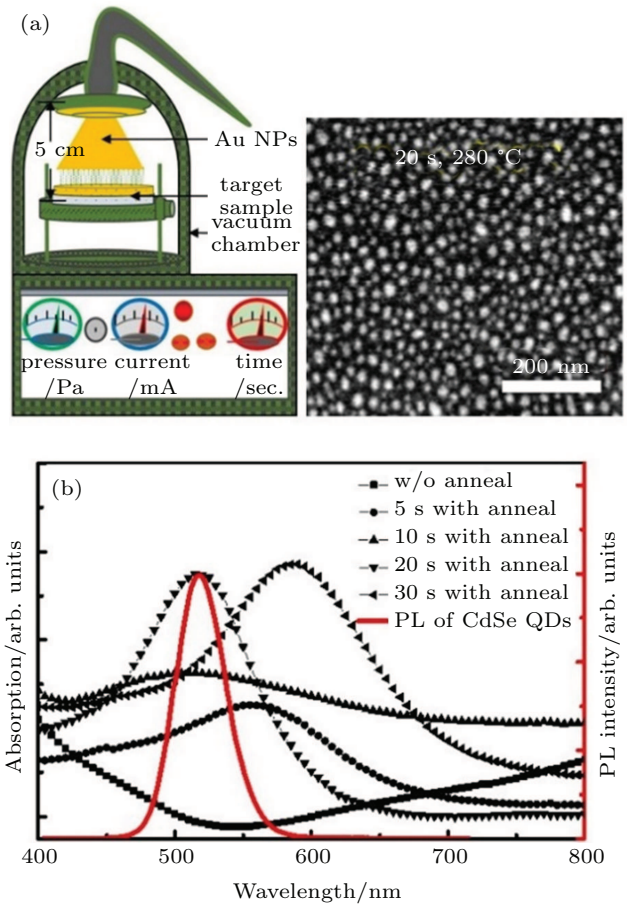


Fig. 1. (color online) (a) Schematic diagram of sputtering machine and SEM micrograph of Au NP film, (b) plots of absorption versus wavelength of different size Au NPs, and plot of PL intensity versus wavelength of CdSe QDs. The w/o means with and without something.

To incorporate the Au plasmonic layer into the electroluminescent quantum dot light emitting diode device, all-solution processed inverted device structure of ITO/Au NPs/ZnMgO/QDs/TFB/PEDOT:PSS/Al is used as shown in Fig. 2(a), where ZnMgO is used as an electron transport layer and also acts as a dielectric spacer layer between Au NP and QDs, which diminishes non-radiative quenching induced by SPs.[26–29] Figure 2(b) depicts an energy level diagram, according to which, the PEDOT:PSS and TFB act as hole injecting and hole transport layers, respectively. Figure 2(c) shows the PL spectra of Au/ZnMgO/QDs and ZnMgO/QDs films, and the PL intensity for plasmonic enhanced QD film is enhanced by 1.7 fold as compared with that of pure QD films, signifying the enhanced spontaneous emission through SP coupling. In order to clarify the origin of PL intensity enhancement in Au NPs' existence, we perform TRPL measurements for QD films coated over pure ZnMgO and Au

NP/ZnMgO substrates respectively, the corresponding decay for both films are shown in Fig. 2(d). It has been revealed that excitons couple to SPs more rapidly than spontaneous recombination of excitons.[30,31] By the incorporation of Au NPs the lifetime of PL should be reduced. Calculations depict the decay times to be 24.82 ns and 23.38 ns for normal quantum dot film and plasmonic quantum dot film, respectively. Reduction in the decay time is related to the increase in exciton coupling, resulting in enhanced quantum dot emission.[32] This new form of recombination, in which electron–hole pairs (excitons) couple to vibrating electrons on the surface of metal to produce SPs instead of phonons or photons, accelerates the spontaneous radiative emission rate and internal quantum efficiencies.[19,33]

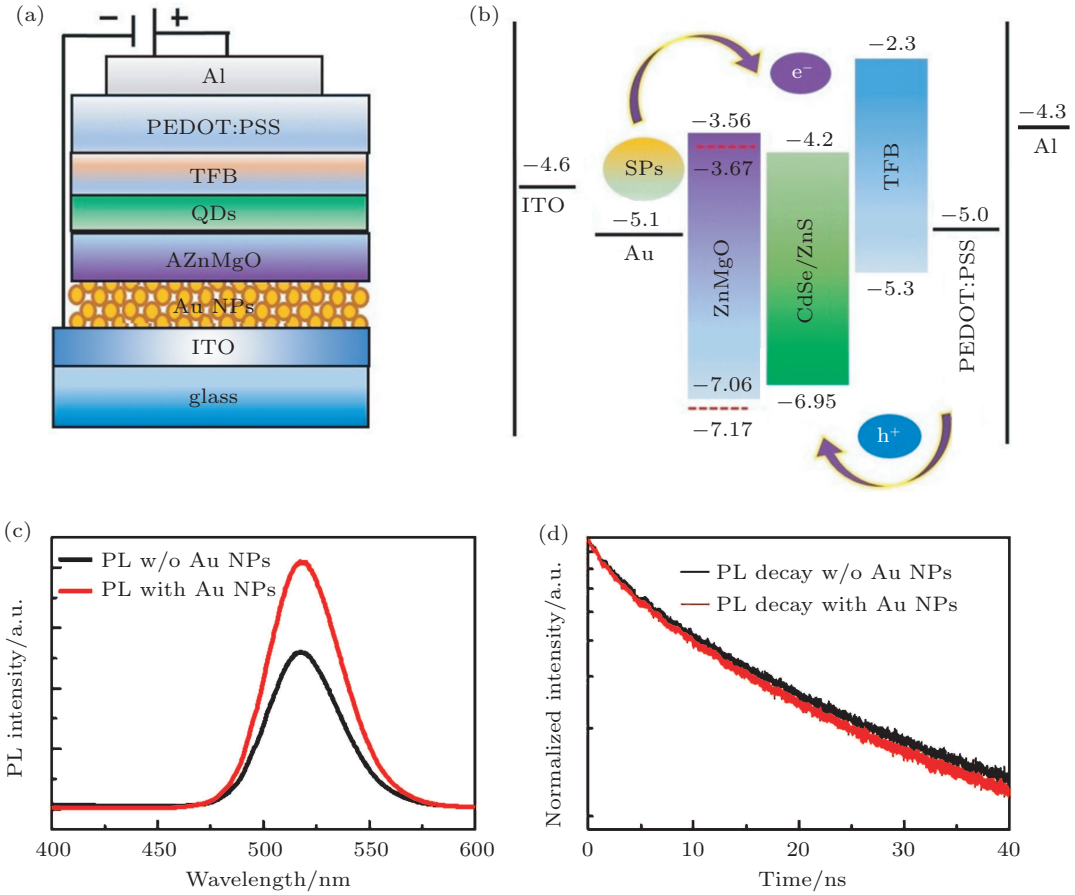


Fig. 2. (color online) (a) Illustration of device structure, (b) energy level diagram, (c) PL intensities of normal and plasmonic substrates, and (d) PL decay behavior of normal and plasmonic substrate.

Half normal/half plasmonic device is fabricated on the same substrate to diminish the systematic error among different batches of devices, which is shown in Fig. 3(a). A comparison of image between normal and plasmonic devices driven at 5 V is also presented. Figure S2 in Appendix A shows normalized EL and PL emissions at the same peak wavelength of 518 nm. Luminance–voltage, current density–voltage characteristics of the normal and plasmonic devices are displayed in Fig. 3(b). The plasmonic device displays the highest luminance of 20720 cd/cm^2, i.e., 1.41 folds larger than that of a normal device. A maximum current efficiency of 4.02 cd/A for a plasmonic device is obtained (Fig. 3(c)), which is improved by 1.29 folds from the normal device. The improvement of current efficiency can be ascribed to the internal field enhancement in the presence of Au NPs due to resonance coupling and fast injection of charge carriers, which ultimately leads to more balanced charge injection. As a result, the turn-on voltage of the plasmonic device is reduced from 3 V to 2.8 V.

The TREL is performed to elaborate the transportation of charge carriers under the effect of Au NPs (Fig. S3 in Appendix A). Transient evolution profiles of normalized electroluminescence (EL) are obtained under a 5-μs pulse with a pulse cycle of 1 ms. Due to low power per pulse, a relatively high applied voltage of 7.5 V is used to yield a measurable luminance of the device. It is observed that EL evolution profiles of normal and plasmonic devices each experience a delay period first, which is followed by a fast rise due to enhanced spontaneous emission and finally overtaken by a slow rise until it reaches to its maximum value. It is clearly seen from the comparison of EL evolution profiles between plasmonic and normal devices that the normal device takes a longer delay and shows a slower initial rise and experiences longer time lag in reaching the maximum EL than the plasmonic device.[33]

A mobility determination technique was used, which is based on a phenomenological numerical model.[33] From the plots of normalized $\{[\mathrm{EL}(t\to\infty)-\mathrm{EL}(t)\,/\mathrm{EL}(t\to\infty)]\}$ versus time and EL versus time (Fig. 4(a)), delay time t_d is defined as the intersection between the horizontal axis and the first slope of the curve, initial rise time t_1 is the time where the first slope and the second slope of the curve intersect, and t_2 is the time when the EL intensity reaches 95% of its steady value.

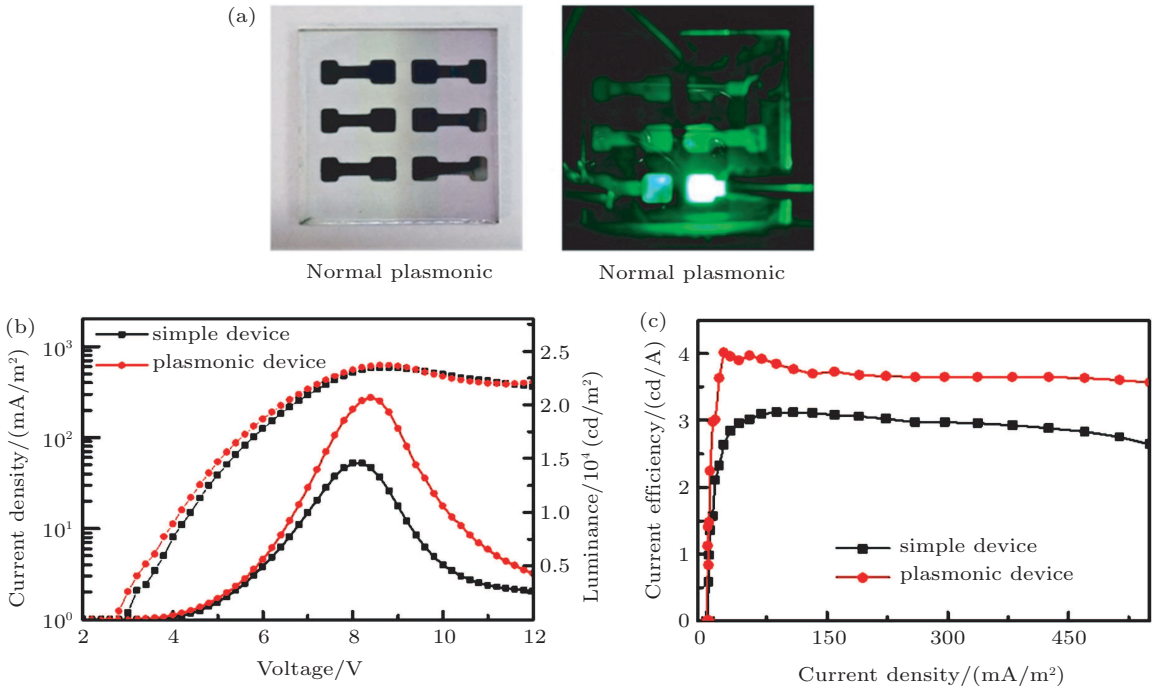


Fig. 3. (color online) (a) Optical image of half normal plasmonic device and half plasmonic device on the same substrate before being on and after lighting, (b) luminance and current density varying with applied voltage for simple and plasmonic devices, and (c) comparison of current efficiency versus current density between two devices.

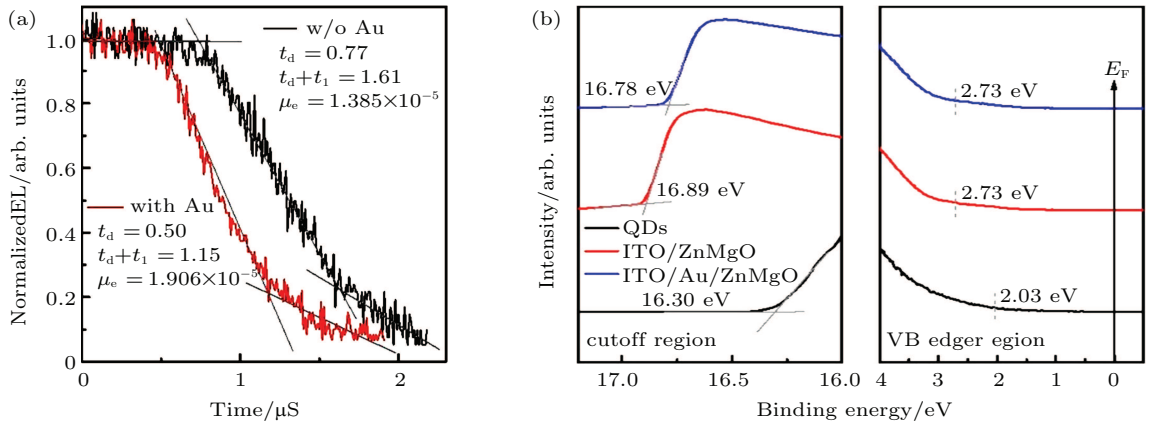


Fig. 4. (color online) (a) Plots of simulated normalized EL versus time from a phenomenological model, and (b) UPS spectrum of QD, ZnMgO, and Au NP enhanced ZnMgO film.

We assume that $\mu_\mathrm{h}\approx\mu_\mathrm{e}$, and taking time measurements t_d, t_1, and t_2 from our experimental measurements we use the equation $\mu_\mathrm{e}=L^2/(V-V_\mathrm{bi})(t_\mathrm{d}+t_1)$ to calculate the mobility of electrons,[33] where V_bi is assumed to be built in the voltage of the device, taken from the difference in work function of ITO between Au NPs and ZnMgO NPs (1.04 V and 0.93 V for normal and plasmonic devices, respectively) and L is the thickness of the device (120 nm).

UPS spectra of ITO/ZnMgO and ITO/Au/ZnMgO are shown in Fig. 4(b). All the spectra are measured using He Iα photons ($h\upsilon$ = 21.22 eV). The lowest occupied molecular orbital (LOMO) energy levels calculated from UPS characteristics (Table S1 in Appendix A) show a 0.11-eV decrement for the ITO/Au/ZnMgO film as compared with that for the ITO/ZnMgO film. Therefore, the charge injection barrier between the ZnMgO and QDs is reduced with Au incorporation and such a reduction consequently contributes to the balanced transportation of carriers across the QDs' layer. As a result, delay time t_d is shortened by 0.27 μs for a plasmonic device compared with for a normal device, manifesting faster

injection of charge carriers from the charge transfer layers into QDs.

Table 1. Characteristic times t_d, t_1, t_2, and electron mobility μ_e.

Normalized EL	t_d/μs	t_1/μs	t_2/μs	μ_e/(cm^2/V·s)
W/O Au	0.77	0.84	2.05	1.39×10^{-5}
With Au	0.50	0.65	1.65	1.91×10^{-5}

The time for the initial rise, t_1 is shortened by 0.19 μs for the plasmonic device. This can be attributed to the efficient resonance coupling of excitons to SPs, which in turn speeds up the spontaneous emission by continuously balancing the flow of carriers in this region. Therefore, the emission process is also accelerated by resonance coupling to produce a brighter emission peak. The comparison of t_2 reveals that the plasmonic device reaches to 95% of its steady EL intensity 0.4 μs faster than the normal device. This consistent behavior of EL evolution holds under our assumption of $\mu_h \approx \mu_e$ across the device. Due to this balance in transportation of charge carriers, mobility enhancement from 1.39×10^{-5} cm^2/V·s to 1.91×10^{-5} cm^2/V·s for Au NPs contained in the device has been achieved. The *I*–*V* traces of the devices comply with the Mott–Gurney power law (Fig. S4 in Appendix A) with an Ohmic region at the lower bias and a space charge-limited current (SCLC) regime at the higher bias. For a plasmonic device, the Ohmic region is observed to be shorter than those for the normal devices, which signifies more rapid carrier transportation, efficient resonance coupling enhanced spontaneous emission, and reduced quenching of excitons under the influence of the plasmonic effect. Furthermore, electron-only devices with the structure of ITO/ZnMgO/QDs/Al and ITO/Au NPs/ZnMgO/QDs/Al are fabricated, and the corresponding current density of the latter with Au NPs is higher than that of the former (Fig. S5 in Appendix A), demonstrating an improved charge injection rate from the charge transport layer to QDs. Combined with the TREL results, the reduced time delay and efficient transportation result in the balance and smooth transportation of carriers in plasmonic devices.

4. Conclusions and perspectives

In this research, we have elaborated SP-enhanced QD-LEDs using Au NPs. Enhancements in the device performance are attributed to the increased charge injection rates into QDs, balanced transportation of carriers across the device, and the strong resonance coupling of SPs and excitons, verified by TRPL, TREL, UPS, and phenomenological numerical results. Enhancement in carrier mobility from 1.39×10^{-5} cm^2/V·s to 1.91×10^{-5} cm^2/V·s verifies the improvement in transportation of charge carriers. Based on the Au incorporation, efficient green emission QD-LEDs each with a maximum luminance of 20700 cd/m^2 and a maximum current efficiency of 4.02 cd/A are achieved. These results demonstrate an effective method to use plasmonic metal nanostructures for achieving super bright and efficient solid-state light emitting devices.

Acknowledgment

The authors thank the BOE Technology Group Co., Ltd. for providing quantum dot samples.

Appendix A: Supporting information

In order to better understand this article, some supporting information is shown in the following table and figures.

Table S1. Work function calculations by UPS measurements.

Sample	Fermi energy(E_F)/eV	Cut off K.E(E_{cutoff})/eV	$\phi = h\nu - (E_{cut\ off} - E_F)$ $h\nu = 21.22$ eV	VB level/eV	CB level/eV
QD	0	16.30	4.92	−6.95	−4.2
ITO/ZnMgO	0	16.89	4.33	−7.06	−3.56
ITO/Au/ZnMgO	0	16.78	4.44	−7.17	−3.67

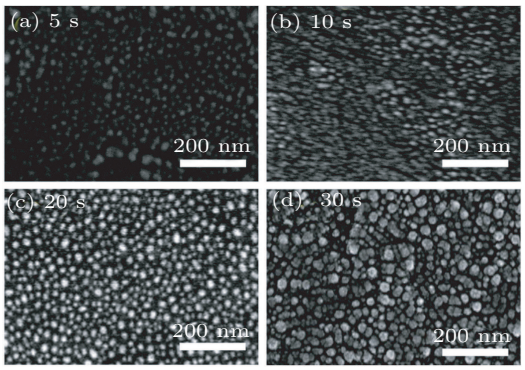


Fig. S1. (color online) SEM micrographs of Au sputtered from 5-cm height for (a) 5 s, (b) 10 s, (c) 20 s, and (d) 30 s, and annealed at 280 °C. The average sizes of Au NPs for different sputtering times and heights are calculated by Image J software to be 12 nm, 13.5 nm, 22 nm, and 35 nm.

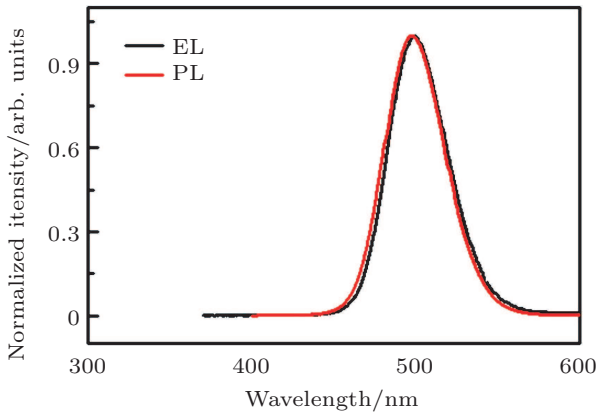


Fig. S2. (color online) Comparison of normalized intensity versus wavelength between two devices.

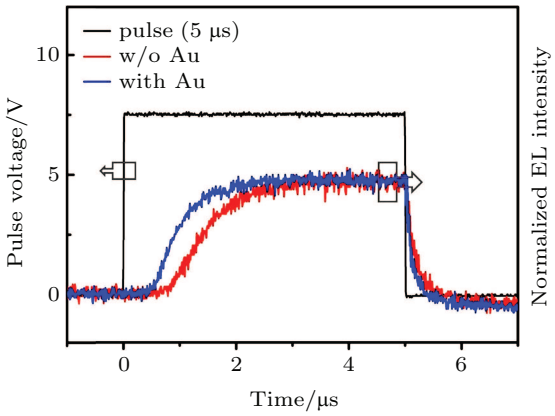


Fig. S3. (color online) Experimental results for pulse voltage and normalized EL intensity varying with time for simple and plasmonic devices under 5-μs pulse voltage.

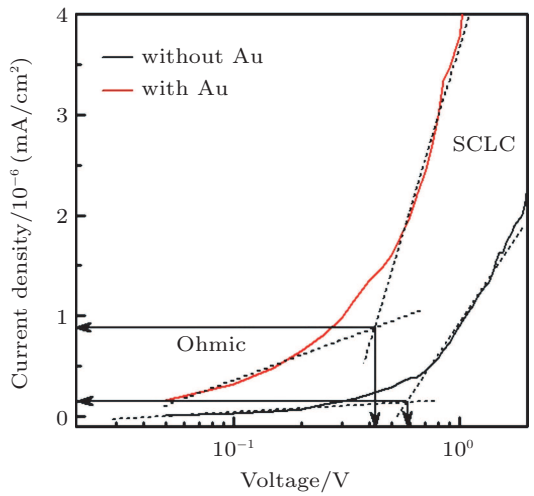


Fig. S4. (color online) Plots of current density versus applied voltage for simple and plasmonic devices at voltages ranging from 0.01 V to 2 V.

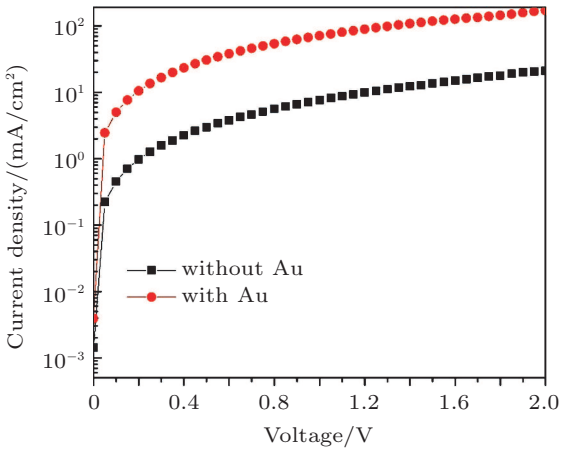


Fig. S5. (color online) Plots of current density versus applied voltage for electron-only devices with structure of ITO/ZnMgO/QDs/Al and ITO/Au NPs/ZnMgO/QDs/Al.

References

[1] Dai X, Deng Y, Peng X and Jin Y 2017 *Adv. Mater.* **29** 07022

[2] Gong X, Yang Z, Walters G, Comin R, Ning Z, Beauregard E, Adinolfi V, Vozny O and Sargent E H 2016 *Nat. Photon.* **1** 11

[3] Ji W, Wang T, Zhu B, Zhang H, Wang R, Zhang D, Chen L, Yang Q and Zhang H 2017 *J. Mater. Chem. C* **5** 00514

[4] Cao F, Wang H, Shen P, Li X, Zheng Y, Shang Y, Zhang J, Ning Z and Yang X 2017 *Adv. Mater.* **27** 04278

[5] Chang S, Zhang X, Wang Z W, Han D B, Tang J L, Bai Z and Zhong H Z *IEEE J. Selec. Top. Quantum Electron* **27** 2688706

[6] Persano L, Catellani A, Dagdeviren C, Ma Y, Guo X, Huang Y, Calzolari A and Pisignano D 2016 *Adv. Mater.* **28** 06381

[7] Yu R, Yin F Huanga X and Ji W 2017 *J. Mater. Chem.* **5** 0514

[8] Pan J, Chen J, Zhao D, Huang Q, Khan Q, Liu X, Tao Z, Zhang Z and Lei W 2016 *Opt. Express* **24** 000A33

[9] Chuang S H and Wuu D S 2015 *SPIE* **5** 005949

[10] Shen H, Cao W, Shewmon N T, Yang C, Li L S and Xue J 2015 *Nano Lett.* **15** 1211

[11] Zaiats G, Ikeda S, Kinge S and Kamat P V 2017 *ACS Appl. Mater. Interfaces* **9** 07893

[12] Wang W, Peng H and Chen S 2016 *J. Mater. Chem. C* **4** 04223

[13] Castan A, Kim H M and Jang J 2014 *ACS Appl. Mater. Interfaces* **6** 04876

[14] Rad A G, Abbasi H and Afzali M H *Phys. Proc.* **22** 032

[15] Kwak J, Bae W K, Lee D, Park I, Lim J, Park M, Cho H, Woo H, Voon D V, Char K and Lee S 2012 *Nano Lett.* **12** 3003254

[16] Heo M, Cho H, Jung J W, Jeong J R, Park S and Kim J Y 2011 *Adv. Mater.* **23** 5689

[17] Shirasaki Y, Supran G J, Bawendi M G and Bulovic V 2013 *Nat. Photon.* **7** 328

[18] Brogersma M L and Kik P G 2007 *Surface Plasmon Nanophotonics* (New York: Springer)

[19] Okamoto K, Wang Z M and Neogi A 2010 *Nanoscale Photonics and Optoelectronics* (Springer Science, Japan)

[20] Wang H, L-Van Q, Assime A, Roux X L, Charra F, Chauvin N and Degiron A 2017 *Adv. Opt. Mater.* **17** 00658

[21] Ji W, Jing P and Zhao J 2013 *J. Mater. Chem. C* **1** 470

[22] Zhang X, Marocico C A, Lunz M, Gerard V A Gunko Y K, Lesnyak V, Gaponik N, Sucha A S, Rogach A L and Bradley A L 2014 *ACS Nano* **8** 1273

[23] Kvitek O, Seigel J, Hunatowio V and Svorik V 2013 *J. Nanomaterials* **1** 743684

[24] Lu L, Luo Z, Xu T and Yu L 2013 *Nano Lett.* **13** 59

[25] Shaojian H, Jun L and Zhanao T 2013 *Prog. Phys.* **33** 0542

[26] Stouwdam J W and Janssen R A J 2008 *J. Mater. Chem.* **18** 1889

[27] Hines M A and Sionnest P G 1996 *J. Phys. Chem.* **100** 468

[28] Qian L, Zheng Y, Xue J and Holloway P H 2011 *Nat. Photon.* **5** 543

[29] Shen H, Lin Q, Cao W, Yang C, Shewmon N T, Wang H, Niu J, Li L S and Xue J 2017 *Nano Lett.* **9** 13583

[30] Bae W K, Lim J, Lee D, Park M, Lee H, Kwak J, Char K, Lee C and Lee S 2014 *Adv. Mater.* **4** 00139

[31] Wang Z, Chen Z, Lan Z, Zhai X Du W and Gong Q 2007 *Appl. Phys. Lett.* **90** 151119

[32] Kim N Y, Hong S H, Kang J W, Myoung N S, Yim S Y, Jung S, Lee K, Tu C W and Park S J 2015 *RSC Adv.* **5** 15585

[33] Pinner D J, Friend R H and Tessler N 1999 *J. Appl. Phys.* **86** 371488